Dalton Transactions

Proton-controlled Non-exponential Photoluminescence in a PyridylAmidine-substituted Re(I) complex

Journal:	*Dalton Transactions*
Manuscript ID	DT-ART-04-2021-001132.R1
Article Type:	Paper
Date Submitted by the Author:	28-Apr-2021
Complete List of Authors:	Martin, Shea; Lehigh University, Department of Chemisry Oldacre, Amanda; Saint Lawrence University, Department of Chemistry Pointer, Craig; Lehigh University, Department of Chemisry Huang, Tao; Lehigh University, Department of Chemisry Repa, Gil; Lehigh University, Department of Chemisry Fredin, Lisa; Lehigh University, Department of Chemisry Young, Elizabeth; Lehigh University, Department of Chemistry

Proton-controlled Non-exponential Photoluminescence in a PyridylAmidine-substituted Re(I) complex.

Shea M. Martin[b], Amanda N. Oldacre[a], Craig A. Pointer[b], Tao Huang[b], Gil M. Repa[b], Lisa A. Fredin[b], and Elizabeth R. Young[b,*]

[a] Department of Chemistry, St. Lawrence University, Canton, New York, 13617, USA.

[b] Department of Chemistry, Lehigh University, Bethlehem, Pennsylvania 18015, USA.

* Email: ery317@lehigh.edu; Fax: +1-610-758-6536.

KEYWORDS. Non-exponential photoluminescence, excited-state proton-coupled electron transfer, excited-state potential energy surfaces, density functional theory, d^6 transition metal complex, rhenium(I) complex.

ABSTRACT: Chemical intuition and well-known design principles can typically be used to create ligand environments in transition metal complexes to deliberately tune reactivity for desired applications. However, intelligent ligand design does not always result in the expected outcomes. Herein we report the synthesis and characterization of a tricarbonyl rhenium (2,2'-bipyridine) 4-pyridylamidine, Re(4-Pam), complex with unexpected photophysical properties. Photoluminescence kinetics of Re(4-Pam) undergoes non-exponential decay, which can be deconvoluted into two emission lifetimes. However, upon protonation of the amidine functionality of the 4-pyridylamidine to form Re(4-PamH) a single exponential decay is observed. To understand and rationalize these experimental observations, density functional theory (DFT) and time-dependent density function theory (TDDFT) are employed. The symmetry or asymmetry of the protonated or deprotonated 4-pyridylamidine ligand, respectively, is the key factor in switching between one and two photoluminescence lifetimes. Specifically, rotation of the dihedral angle formed between the bipyridine and 4-Pam ligand leads to two rotamers of Re(4-Pam) with degenerate triplet- to ground-state transitions.

INTRODUCTION

Inorganic chemists oftentimes take advantage of multifaceted ligand environments to tune the reactivity of metal complexes for their desired applications from photoredox catalysis to ion sensing.[1–3] In order to establish the design principles to achieve desired tunability, fundamental research must be used to reveal the underlying molecular trends imparted by the ligand environment. The d^6 transition metal complexes have been extensively studied.[4] These complexes possess potential triplet metal-to-ligand charge transfer (^{3}MLCT) excited states that have shown intriguing long-lived excited states and good photo-stability making them ideal for photo-induced chemical reactions.

Some of the most iconic of these d^6 transition metal complexes are ruthenium(II) trisbipyridine-based (Ru(II)bpy$_3$) complexes. Ru(II)bpy$_3$ complexes have a rich history in photochemistry and photoredox catalysis because they are photostable and the bipyridine ligand can be used to tune the ligand environment around the metal center thereby imparting desired photochemical properties to the complex.[5,6] Ru(II)bpy$_3$ undergoes a ^{1}MLCT transition upon excitation, and very rapidly (sub-picosecond) undergoes intersystem crossing to form the ^{3}MLCT excited state, which lives for several hundred nanoseconds. Fundamental studies of Ru(II)bpy$_3$ and other d^6 transition metal complexes have demonstrated that charge-transfer electron density localizes on the lowest lying ligand π^* orbital of the ligand rather than delocalizing over all available ligand orbitals.[7] Further, if different ligands, or differently substituted bipyridine ligands are used to synthesize transition metal complexes, the localization of the MLCT excited state can be purposefully dialed onto (or away from) a particular ligand by considering the relative electronic stability of the individual bipyridine ligand.[8–11] From foundational, fundamental work on d^6 transition metal complexes, inorganic chemists have continued to develop chemical intuition through

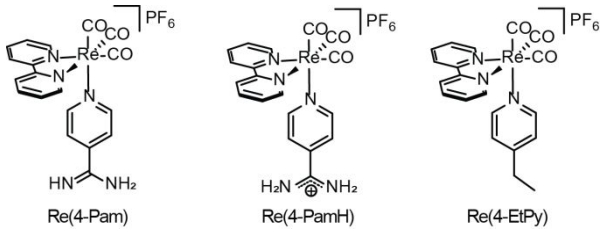

Figure 1. Re(4-Pam), Re(4-PamH) and Re(4-EtPy) complexes.

fundamental research that is critical in designing d^6 transition metal complexes to suit their various needs.

Our lab is interested in exploring new reaction pathways to utilize ^{3}MLCT excited states that promote proton-coupled electron-transfer (PCET) reactivities for renewable-energy relevant applications. Towards this end, we recently set out to design and synthesize a new photoreductant for a photo-induced PCET model system. In doing so, we synthesized a tricarbonyl rhenium (2,2'-bipyridine) 4-pyridylamidine, Re(4-Pam), complex (Figure 1). Re(I) carbonyl complexes[12–20] are known to possess large photo-reduction potentials because of the highly electron-withdrawing nature of the carbonyl ligands[10,21]. The 4-pyridyl amidine ligand was employed to serve as the protonic-sensitive component of the complex.

Table 1. Summary of Absorption and Emission Maxima and Redox Potentials

	Absorption (nm)	Emission (nm)	$E_{1/2}$ (ox) (V vs. Fc/Fc^+)	$E_{1/2}$ (red) (V vs. Fc/Fc^+)
Re(4-Pam)	242, 307, 318 (sharp), 350	555	1.20	–1.60, –1.79
Re(4-PamH)	245 (shoulder), 266 (shoulder), 305, 317 (sharp), 350 (shoulder)	555	1.20	–1.59
Re(4-EtPy)	243 (shoulder), 293, 318 (sharp), 360	550	1.20	–1.58

All data are collected and reported in dried dicholoromethane. Electrochemistry is performed with 0.10 M tetrabutylammonium hexafluorophospate. The sharp peak at 318 nm does not correspond to lamp crossover.

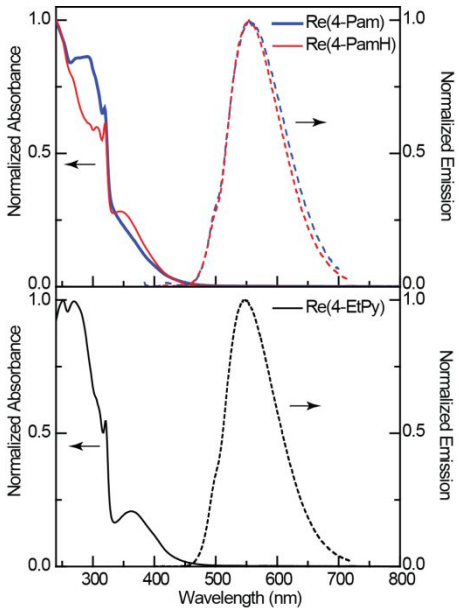

Figure 2. Normalized UV-visible absorption and emission spectra of (top) Re(4-Pam), bold blue, and Re(4-PamH), thin red, and (bottom) Re(4-EtPy) in dichloromethane.

In the process of characterizing Re(4-Pam), we were surprised to find that the photoluminescence kinetics of Re(4-Pam) undergoes non-exponential decay, which can deconvolved into two emission lifetimes. The influence of emitting impurities has been ruled out by IR (Figure S1) and NMR (Figure S2) spectroscopic analysis, together with transient absorption spectroscopy. Transient absorption spectroscopy, which is not susceptible to highly emissive trace impurities, confirmed the observation of non-exponential decay lifetimes obtained by the photoluminescence lifetime fitting.

Non-exponential decay kinetics have been observed in analogous Re complexes[22,23] and other systems[24–31] and have been attributed to a wide range of photophysical processes, including dual emission, environmental heterogeneity or structural isomer effects. Dual emission has been extensively studied in several analogous d^6 Ru transition metal complexes.[29–33] Dual emission has been attributed to the presence of multiple, *non-equilibrated* emissive states that are most prominently observed in complexes containing asymmetric ligands.[31,33] This type of dual emission is often characterized by the observation of two or more distinct emission features in the steady-state emission spectrum that occur because the two distinct states exist at different energies relative to the ground state. Environmental heterogeneity is also known to result in non-exponential photoluminescence, however, this is primarily observed in solid-state systems.[28,34] Finally, the existence of ground-state structural isomers may rationalize the observation of non-exponential photoluminescence. For example, tryptophan shows non-exponential decay kinetics stemming from two different ground-state rotamers. Each rotamer undergoes different electron transfer kinetics from the indole to nearby electrophiles due to the change in electron transfer distance.[25,35] While there have been reports of non-exponential photoluminescence for the d^6 Re system, the reason behind this behavior has not been well explained or rationalized.[22]

As part of our efforts to understand Re(4-Pam), we protonated the amidine functionality to form Re(4-PamH). Additionally, we prepared an analogous compound that has no protonation site, by replacing the 4-Pam ligand with a 4-ethylpyridine ligand (4-EtPy) to create Re(4-EtPy). Re(4-EtPy) has been previously isolated and reported by Meyer *et. al.*[10], and is known to have only one emission lifetime as reported by McCusker *et. al.*[36]

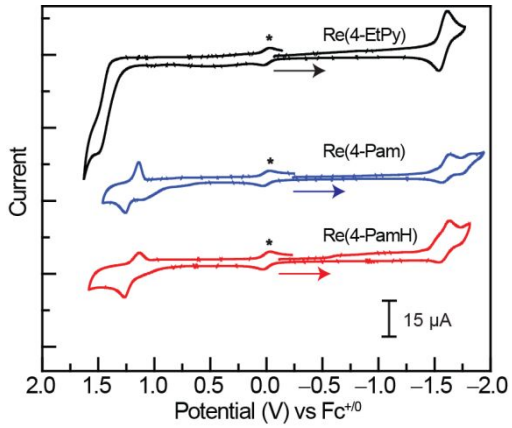

Figure 3. Cyclic voltammograms of Re(4-EtPy), Re(4-Pam) and Re(4-PamH) in dichloromethane (0.100 M electrolyte). Samples were degassed for 10 min prior to measurement and an N_2 blanket was used throughout the experiment. Peaks at 0.0 V indicated with an asterisks are the ferrocene couple used as the internal reference.

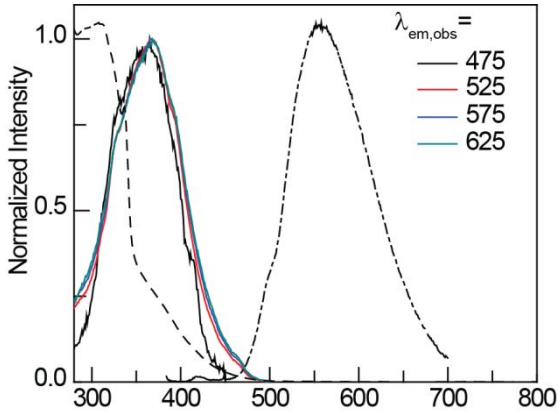

Figure 4. Excitation spectra of Re(4-Pam) in dicholoromethane. The emission was recorded at the indicated wavelength as the excitation wavelength was scanned from 290-500 nm (solid lines). Dashed line represents the absorption spectrum and the dash-dotted line represents the emission spectrum of Re(4-Pam).

Density functional theory (DFT) and time-dependent DFT (TDDFT) calculations were employed to shed light on the excited-state manifolds of these model molecules. We found that there is a critical, geometric coordinate in Re(4-Pam), specifically, rotation of the dihedral angle formed between the bipyridine and 4-Pam ligand that leads to two rotamers with degenerate triplet- to ground-state transitions.

RESULTS AND DISCUSSION

Synthesis: Re(4-Pam), Re(4-PamH) and Re(4-EtPy) are shown in Figure 1. Re(4-EtPy) was prepared using literature procedures.[10,36] Briefly, 37 equivalents of 4-EtPy were added to a solution of acetonitrile adduct of the starting material, which was refluxed overnight. Re(4-Pam) was prepared by two distinct methods: (1) refluxing 10 eq of 4-Pam with a DMSO adduct of $[Re(bpy)(CO)_3(o\text{-}DMSO)]PF_6$ in THF overnight to produce a PF_6 salt of the product Re(4-Pam) or (2) refluxing equimolar $Re(bpy)(CO)_3Cl$, 4-Pam and sodium tetrakis[3,5-bis(trifluoromethyl)phenyl]borate (Na(BArF)) for 72 hours in 1,2-difluorobenzene to produce a BArF salt of the complex (Re(4-Pam BArF)). All spectroscopic data reported in the main text are reported for the PF_6 salt, which is called Re(4-Pam) in this report. When comparison to the BArF salt is needed, Re(4-Pam BArF) will be used to denote the BArF counter ion complex. Re(4-EtPy) and Re(4-Pam) were isolated and NMR and ESI-MS were used to confirm the desired product was obtained (Figure S2). To obtain the protonated analogue of Re(4-Pam), Re(4-PamH), ~ 2 mol equivalents of protonated dimethylformamide (HDMF)[37,38] were added to samples containing Re(4-Pam) *in situ* and experimental characterization was carried out. The non-exponential decay kinetics (*vide infra*) observed for Re(4-Pam) were recorded on the products obtained of each synthesis method.

UV-visible absorption spectroscopy: UV-visible absorption spectra of each complex are shown in Figure 2 and summarized in Table 1. Re(4-Pam) shows intense absorption below 325 nm due to ligand-centered transitions associated with the bipyridine and 4-pyridyl amidine ligands. A shoulder centered at ~350 nm represents the metal-to-ligand charge transfer transition in Re(4-Pam). The protonated form of the complex, Re(4-PamH), shows absorption associated with the ligand-centered transitions (between 250 – 325 nm) that decreases in intensity relative to the absorption feature representing the metal-to-ligand charge transfer transition (centered at 350 nm), which becomes more prominent and resolved. The red shift in the absorption spectrum of Re(4-PamH) occurs because of the stabilization of the 4-pyridyl amidine ligand in the protonated form as will be discussed in the computational section (*vide infra*). The absorption spectra of Re(4-EtPy) resembles the absorption spectra of Re(4-Pam) and Re(4-PamH) and match well with literature reports of the complex.[10,36]

Emission spectroscopy: Emission spectra of Re(4-Pam), Re(4-PamH) and Re(4-EtPy) are shown in Figure 2. The emission spectra of Re(4-Pam) and Re(4-PamH) both show a peak at 555 nm and are essentially unperturbed by the presence or absence of the proton on the amidine functionality. The emission spectrum of Re(4-EtPy) shows a broad peak at 550 nm that resembles those of the Re(4-Pam) and Re(4-PamH) and is consistent with literature reports.

Electrochemistry: Cyclic voltammetry (CV) of Re(4-Pam), Re(4-PamH) and Re(4-EtPy) are shown in Figure 3 and summarized in Table 1. A reversible reduction peak is observed at ~ −1.59 V vs. $Fc^{+/0}$ corresponding to reduction of the bipyridine ligand. A second reduction peak is observed at −1.79 for only the Re(4-Pam) corresponding to the 4-pyridylamidine. Quasi-reversible oxidation peaks are observed for Re(4-Pam) and Re(4-PamH) at 1.20 V vs. $Fc^{+/0}$ and an irreversible oxidation peak at 1.53 V vs. $Fc^{+/0}$ is observed for Re(4-EtPy) corresponding to oxidation of the Re metal center. Re(4-Pam) and Re(4-PamH) show similar oxidation potentials as both are $Re^{2+/+}$ couples with identical Re d_π orbital energies (*vide infra*). On the other hand, the observed shift of 0.33 V of Re(4-EtPy) $Re^{2+/+}$ couple indicates that the oxidation of Re(4-EtPy) is more difficult than the oxidation of the Re(4-Pam) or Re(4-PamH). This shift could be attributed to the electron donating ability of the ethyl group versus the amidine functionality. The amidine functionality is a stronger electron donating group on the pyridine ring, which in turn donates to the Re metal center and makes the Re(4-Pam) and Re(4-PamH) easier to oxidize.

Table 2. Ambient Temperature Time-resolved Emission and Transient Absorption Spectroscopy Lifetimes

	Time-resolved Emission[#]		Transient Absorption Lifetimes		
	τ_1(Ampl[§]) (ns)	τ_2(Ampl[§]) (ns)	τ_{short} (ps)	τ_1(Ampl[§]) (ns)	τ_1(Ampl[§]) (ns)
Re(4-Pam)	23 ± 8 (44)	80 ± 30 (56)	67 ± 17	32 ± 4 (82)	77 ±17 (18)
Re(4-PamH)	118 ± 21		51 ± 5	198 ± 8	
Re(4-EtPy)	669*		38 ± 10	344 ± 18	

* Value from ref. 10

§ Amplitude of the contribution of each lifetime to the overall signal.

The entire emission is peak is integrated for time-resolved emission lifetimes. Isolating various wavelengths within the peak did not produce wavelength-dependent lifetimes.

All results reported for the PF_6 counter ion.

Time-resolved emission: Table 2 reports the emission lifetimes obtained for each rhenium complex in dichloromethane. Samples were prepared using freeze-pump-thaw techniques in a 1-cm quartz cuvette. Fitting of the time-resolved emission data for Re(4-Pam) yielded unexpected non-exponential behavior. Two emission lifetimes (23 ns, 80ns) were obtained that provided approximately the same contribution to the overall signal. In contrast, fitting of Re(4-PamH) yielded mono-exponential behavior resulting in a lifetime of 118 ns. Figure S14 shows fits of representative Re(4-Pam) and Re(4-PamH) data to both mono- and bi-exponential functions along with the R^2 value and residual trace associated with each fit. The same behavior was observed for Re(4-Pam BArF), the complex in which we switched the counter ion. Unprotonated Re(4-Pam BArF) produced lifetimes of 36 ns ad 234 ns, while protonated Re(4-Pam BArF) produced a single lifetime of 137 ns. Comparison of fitting results for complexes with each counter ion are summarized in Figure S17.

Temperature-dependent time-resolved emission was obtained between 0 and 38 °C for Re(4-Pam). Figure S15 describes the fitting of the temperature-dependent data and presents an Arrhenius plot of the weighted average of the two fitted lifetimes. While the temperature-dependent data contains a high degree of uncertainty (e.g. $R^2 \sim 0.52$ for the non-weighted fit), the general trend provides an indication of the activation barrier for conversion between the two states that participate in the emission process. The slope of the linear fit to an Arrhenius plot is related to the activation energy (E_a) of the emission process by E_a = slope × R. Given the fits, activation energies of 48.4 meV (non-weighted fit) and 67.8 meV (weighted fit) are obtained. The very small value for the activation energy (room temperature is ~ 25 meV, for comparison) indicates that the process being measured possesses a very low activation barrier as we have predicted by DFT (*vide infra*).

Emission excitation spectroscopy: Emission excitation spectra of Re(4-Pam) were acquired to determine if there were two emitting species present in the sample that could be causing observation of two emission lifetimes. Figure 4 shows the excitation spectra for Re(4-Pam) recorded at four emission wavelengths spanning the emission spectrum. The four emission excitation spectra were normalized for comparison and are overlaid with the absorption and emission spectrum of Re(4-Pam). These results show that emission occurs from the lowest energy absorption feature and therefore, the presence of two substantially different emitting species is unlikely.

Further, NMR and IR (Figures S1 and S2) data were carefully analyzed to confirm that only one stereoisomer of Re(4-Pam) was present. Further details are provided in the Supporting Information.

Transient absorption spectroscopy: Because transient absorption spectroscopy is an absorption technique, it is an excellent complement to the emission data presented above. If a highly emissive low-concentration impurity that is present in small concentrations contributed to the emission data, transient absorption spectroscopy will not detect the contribution due to the small absorption of this species. We therefore carried out transient absorption spectroscopy on each rhenium complex to compare the results to the lifetimes obtained by time-resolved emission spectroscopy.

Femtosecond (fs-TA) and nanosecond (ns-TA) transient absorption spectroscopy was carried out on Re(4-Pam), Re(4-PamH) and Re(4-EtPy) (Figure 5). The fs-TA representative spectra for each rhenium complex (Figure 5A, C, E) showed a broad, featureless induced absorption that decayed modestly over the 5.5 ns window of the fs-TA measurement. Global analysis fitting was carried out on the fs-TA data (Figure 5B, D, F) to reveal two decay-associated difference spectra (DADS) for each complex, one with a short (sub-100ps) lifetime and the other with a lifetime that was too long to be fit with the fs-TA data (labeled "Inf").

To assign the lifetime(s) of the second DADS, global analysis fitting of the ns-TA data was carried out and is reported as the lifetime(s) for the second, longer-lived DADS. The lifetimes obtained from nanosecond global analysis fitting are shown in Figure 5 as τ_1 (and τ_2) in blue text below the "Inf" label. ns-TA data is shown as a heat map in Figure S3 to represent the spectral evolution. The low signal-to-noise in ns-TA made it difficult to show the representative spectra directly. Figure S16 shows the time trace of the single principal component obtained from the global analysis fitting of the ns-TA data for both Re(4-PamH) and Re(4-Pam). The single principal component obtained from global analysis was fit to mono- or bi-exponential fits for Re(4-PamH) and mono-, bi-, or tri- exponential fits for Re(4-Pam) using Origin. The results of the fits, their residuals, and the explanation for the fitting process are reported in Figure S16.

For Re(4-Pam), the fs-TA representative spectra (Figure 5A) show a broad, induced absorption around 460 nm that decays very slightly over the 5.5 ns window. The global analysis DADS (Figure 5B) show that this feature is comprised of one low-intensity DADS with a peak centered at 600 nm and a lifetime of 67 ps, and a longer-lived DADS that peaks around 460 nm. This longer-lived DADS was found to consist of two

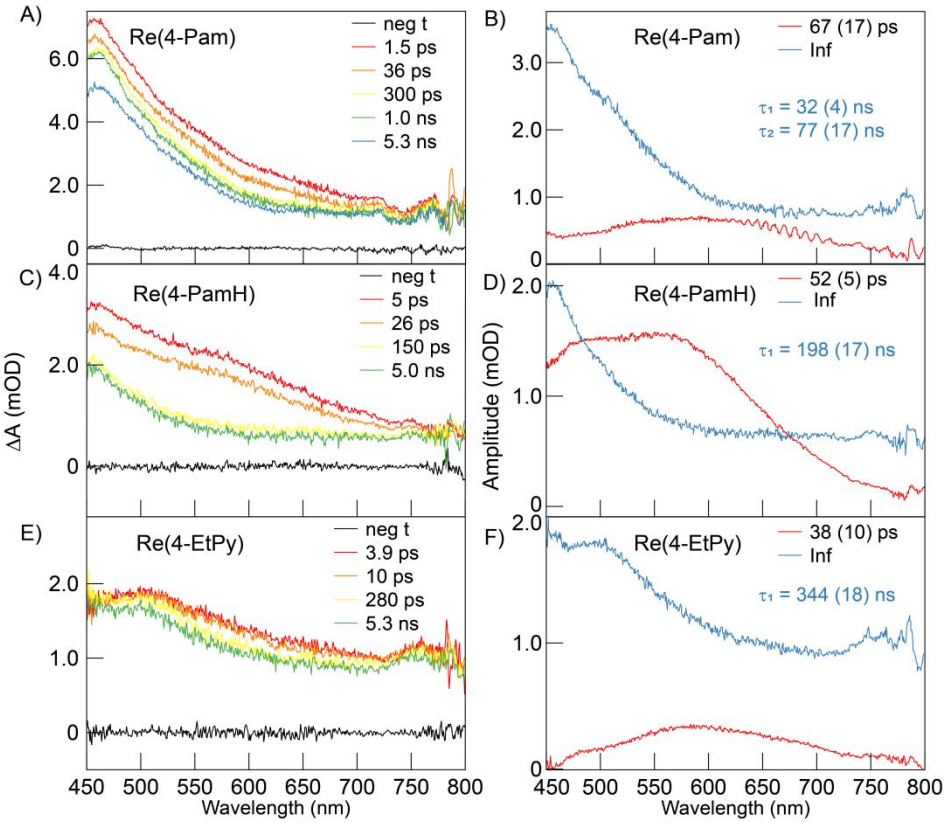

Figure 5. Transient absorption spectroscopy representative spectra (A, C, E) and global analysis decay-associated difference spectra, DADS, (B, D, F) for Re(4-Pam) (A, B), Re(4-PamH) (C, D) and Re(4-EtPy) (E, F). Samples were prepared under high-vacuum conditions in dichloromethane. The Inf DADS represent a lifetime that was too long to fit with the fs-TA system. Lifetimes for the Inf DADS were obtained by global analysis of ns-TA data and are reported as τ_1 and τ_2 in blue.

lifetimes (32 and 77 ns) through global analysis fitting of ns-TA data (Figure S16).

In contrast, the representative spectra of Re(4-PamH) (Figure 5C) decay more substantially over the 5.5 ns window of fs-TA, although not entirely. The DADS of Re(4-PamH) (Figure 5D) show a more significant contribution of the short-lived DADS, which is centered at 550 nm and has a lifetime of 52 ps. The longer-lived DADS appears qualitatively similar in spectral shape to the longer-lived DADS of Re(4-Pam), however, fitting of the ns-TA data shows that this component decays with one lifetime (198 ns) rather than two. Thus, Re(4-Pam) and Re(4-PamH), which differ only by one proton on the amidine/amidinium functionality, show divergent photophysics, likely driven by the change in symmetry of the deprotonated 4-Pam ligand (*vide infra*).

The Re(4-EtPy) was prepared and run as a well-studied analogue to these newly prepared Re(4-Pam) complexes. The fs-representative spectra of Re(4-EtPy) more closely resembles that of the Re(4-Pam) complex. The representative spectra of Re(4-EtPy) (Figure 5E) show a broad induced absorption centered around 500 nm that decays only slightly in the 5.5 ns window of the fs-TA experiment. Global analysis of this data reveals two DADS (Figure 5F). One DADS is relatively weak in intensity, is centered at 600 nm and fits to a lifetime of 38 ps. The second, longer-lived DADS is centered around 500 nm and is found, using fitting of ns-TA data to have a 344 ns lifetime.

The short-lived lifetimes and their corresponding DADS represent the fast singlet to triplet transition of the rhenium complexes. Re(I) tricarbonyl diimine X complexes (where X is among other ligands, Cl, Br, I, pyridine, imidazole) can exhibit intersystem crossing over a wide range of time scales, from ~100 fs, to several ps, to ns-μs time ranges, depending on the nature of the diamine (*i.e.* 2,2-bipyridine or 1,10-phenanthroline) or X ligand.[39] The longer-lived lifetimes represent decay of the triplet state back to the ground state. The bi-exponential decay of the Re(4-Pam) is unexpected in these complexes and indicates a more complex excited-state manifold, which we explore in the *Computational Studies* section below.

Computational Studies: Density functional theory (DFT) was used to calculate the electronic structure of the three rhenium complexes. Restricted and unrestricted DFT were employed to explore the lowest singlet and triplet surfaces and singlet and triplet time-dependent density functional theory (TDDFT) was employed to map the excited-state potential energy surfaces of Re(4-Pam), Re(4-PamH), and Re(4-EtPy).

The frontier molecular orbitals (MOs) (Figure S4 and S5) of Re(4-Pam), Re(4-PamH) and Re(4-EtPy) consist of occupied Re-centered (d_π) (where HOMO is the highest occupied molecular orbital) and unoccupied ligand π^* orbitals (where LUMO is the lowest unoccupied molecular orbital). For Re(4-EtPy), the ligand-centered LUMOs are all primarily bpy with small amounts of electron density on 4-EtPy in the LUMO+1

and LUMO+2, and the HOMOs are Re-centered (d_π). In Re(4-Pam) the LUMO is a bpy centered π* orbital (π^*_{bpy}) and the LUMO+1 is a 4-Pam π* (π^*_{4-Pam}). However, in Re(4-PamH) these two orbitals are reversed and the LUMO, rather than the LUMO+1, is localized on the 4-PamH ligand.

potential energy surfaces to better understand the photophysical behavior of the Re(4-Pam), Re(4-PamH) and Re(4-EtPy). It is important to note that no other geometric coordinate shows significant change across this scan in either the optimized singlets or triplets (Figure S10).

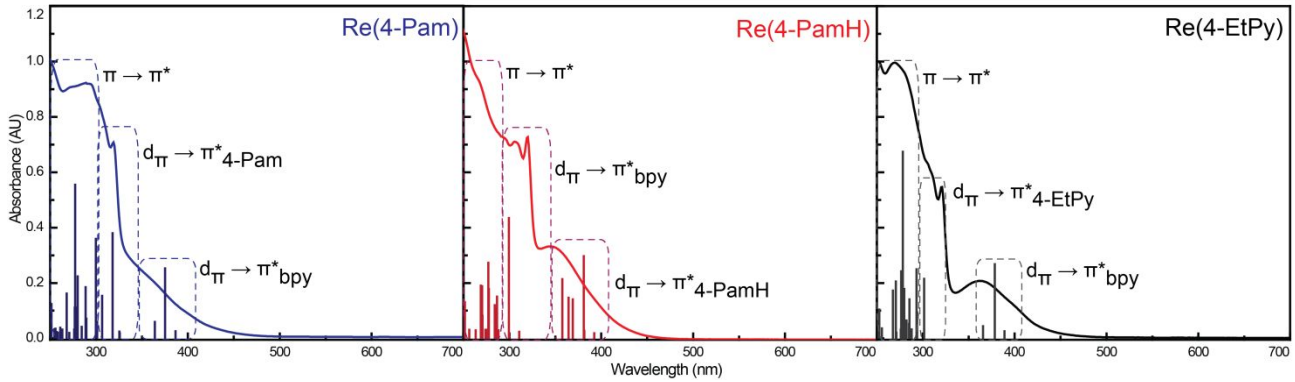

Figure 6. Absorption spectra for Re(4-Pam), Re(4-PamH) and Re(4-EtPy) with the DFT results for absorption transitions. The calculated molecular orbitals of each of the primary transitions is shown from B3LYP/LANL2DZ [Re]+6-311G(d,p)[H,C,N,O]/PCM(ACN).

Protonation of the 4-Pam ligand to produce Re(4-PamH) results in a significant orbital energy stabilization (~ 0.117 eV) of the 4-PamH π* orbital. The energies of the other MOs remain constant between the two molecules, with only the energy of the 4-Pam π* changing (Figure S4). This stabilization of the 4-Pam π* is not unexpected as protonation of amidine makes 4-PamH positively charged and less electron donating. Electron withdrawing groups are known to reduce orbital energies, leading to stabilization of the MO with 4-PamH character.

TDDFT was used to predict the absorption spectrum and identify the corresponding transitions for Re(4-Pam), Re(4-PamH) and Re(4-EtPy) (Figure 6). TDDFT shows that the lowest energy absorption features (λ~350-450 nm) stem from metal-to-ligand charge transfer (MLCT) excitations dominated by Re $d_\pi \rightarrow \pi^*_{bpy}$ transitions. In addition, the reordering of the Re(4-PamH) molecular orbitals leads to some low energy MLCT Re $d_\pi \rightarrow \pi^*_{4-Pam}$ transitions. Higher energy absorption features (λ~250-300 nm) are primarily $\pi \rightarrow \pi^*$ ligand-to-ligand charge transfer excitations.

Computationally exploring the excited-state potential energy surfaces can be invaluable to untangling observed photophysical behavior.[40] Freely optimizing important states of the system, often the ground state (GS) and triplet state (T) for metal centered complexes, provides a picture of the geometric space of interest. DFT optimizations of the lowest energy singlet and triplet for each complex revealed a significant molecular rearrangement between the two states only for Re(4-Pam). Geometric coordinates, such as the length of Re-CO bonds, the angles surrounding the bpy ligand, and the dihedral angles between the pyridine and bpy ligands, were compared to determine the coordinate that changes the most between the two states. Re(4-Pam) shows a significant change in the dihedral angle between the bpy and 4-Pam, comprised of the N(bpy) – Re – N(4-Pam) – C(4-Pam) atoms ($\theta_{dihedral}$) (Figure S5, Figure S6 and Figure 7), of approximately ~90° between the two fully relaxed geometries going from $\theta_{dihedral}$ = –49° in the GS to $\theta_{dihedral}$ = ~40° in the lowest energy triplet (T). Thus this $\theta_{dihedral}$ was chosen as a coordinate over which to scan the excited-state

By constraining only this dihedral ($\theta_{dihedral}$) and optimizing all the other atoms, a potential energy curve (PEC) was mapped along the GS surface (S_0) as a function of the dihedral angle. In each of the S_0s (Figure 7), two minima are observed at $\theta_{dihedral}$ = –49° and 126°. The barrier for rotation between these two geometries is 146.4 meV for Re(4-Pam), 127.1 meV Re(4-PamH) and 48.1 meV for Re(4-EtPy). These barriers are all multiples of kT and only 0.6% of the Maxwell-Boltzmann ensemble would possess energies higher than the barrier at room temperature. Thus each complex GS is dominated by these minima. For Re(4-PamH) and Re(4-EtPy), the two minima on each ground-state surface represent the exact same molecular geometry, while for the Re(4-Pam), the two ground-state surface minima represent two distinctly different geometries that are rotamers of each other. The *molecular* geometries of Re(4-PamH) and Re(4-EtPy) are both symmetrical around $\theta_{dihedral}$, meaning that during the second 180° rotation of the dihedral angle, the molecular geometry repeats the geometries of the first 180° rotation. In contrast, the *molecular* geometry of the Re(4-Pam) is not symmetric around the $\theta_{dihedral}$. The 4-Pam ligand itself is asymmetric owing to the non-protonated amine functionality. Therefore, as the 4-Pam ligand rotates through the dihedral angle, the molecule switches between two distinct rotamers. For example, Figure 1 shows the exo-NH_2 rotamer, in which the configuration of the amine NH_2 is defined relative to the bipyridine ligand of Re(4-Pam). The endo-NH_2 rotamer represents the molecular geometry in which the amine is rotated by 180°. To highlight this difference, Figure 7 shows half of the dihedral angle scan is greyed out for Re(4-PamH) and Re(4-EtPy), while all of the dihedral angle scan remains colored for Re(4-Pam). Further, the two rotamers of Re(4-Pam) are shown above the PECs in Figure 7 with the amidine functionality explicitly drawn out for each half of the dihedral scan.

To rationalize the photophysical behavior of Re(4-Pam), Re(4-PamH), and Re(4-EtPy), we must consider the various pathways the excited complexes can take as they relax back to the ground-state surface. Thus, the TDDFT singlet and triplet excitations were calculated above each S_0 (Figure 7) in order to

map the excited-state decay and emission. Each set of PECs (S_0 and excited states) with transition energies and several barrier heights labeled on the plot are shown in Figures S7, S8 and S9. These electronic PECs map the energy gaps between states at different geometries. To account for spin effects, we also calculated the spin-orbit coupling between singlet and triplet surfaces less than 3.4 eV above the ground state as this represents the system excited under experimental conditions (λ_{ex} = 370 nm).

In general, excitation can be considered to occur from the ground-state surface (S_0) onto an excited singlet-state surface. If excited onto higher energy singlet states, internal conversion to the lowest singlet excited state should be extremely rapid (faster than the temporal resolution of our instrumentation). Once on the first singlet excited-state surface (S_1), rhenium complexes are known to undergo rapid intersystem crossing to triplet states. Intersystem crossing normally occurs at conical intersections (or intersections of surfaces), when there is a small energy gap between surfaces and strong spin-orbit coupling between singlet and triplet. If the triplet surface that results from intersystem crossing is not the lowest lying triplet, then internal conversion should occur to the lowest-lying triplet surface (T_1) in 10s of ps. Importantly, each set of PECs has a clear lowest energy triplet surface that has similar shape to the S_0 with strong spin-orbit coupling between the two surfaces (Table S1-S3).

The differing photophysics observed in these complexes seem to stem from the different number equivalent triplet (T_1) to GS transitions. Either Re(4-Pam) rotamer, *i.e.* the two local minima on the S_0 surface, excited into the singlet manifold should quickly result in population of the lowest energy singlet excited surface, S_1. The S_1 surface intersects with the T_2 and there is strong spin-orbit coupling between S_1 and T_2 ($-52° \leq \theta_{dihedral} \geq 127°$, Figure S11 and Table S1). Once in the triplet manifold, transition state theory:

$$\boldsymbol{\kappa} = \frac{\boldsymbol{k_B T}}{\boldsymbol{h}} \boldsymbol{e}^{-\frac{\boldsymbol{\Delta G^{\ddagger}}}{\boldsymbol{RT}}} \qquad (1)$$

predicts the pyridine rotation on the T_2 and T_1 surfaces (using computed electronic energy barriers on the T_2 and T_1 surfaces as estimates of $\Delta G^{\ddagger}$) to occur in ~ 10 ps which is significantly faster than the emission lifetime and on the order of the triplet internal conversion. Thus the nanosecond emission, should arise from a $T_1 \rightarrow S_0$ transition.

Each T_1 rotamer minimum is ~2.9 eV (2.906 eV for the exo-NH_2 and 2.907 eV for the endo-NH_2 rotamer) above the GS surface, leading to two populations which emit at the same wavelength. Out of an abundance of caution, we calculated the energy of the quintet state to rule out the possibility that the dual emission was coming from an additional intersystem crossing. The fully optimized quintet is 5.2 eV above the GS, which is well outside the excitation window (Figure S12). Thus we propose that the two emission lifetimes arise from different rotamer T_1 populations emitting at the same wavelength.

While the Re(4-PamH) is similarly excited from its GS into the singlet manifold, the excited-state evolution differs slightly from Re(4-Pam). TDDFT of Re(4-PamH) shows a minimum on the S_1 surface directly above the GS. The T_4 surface intersects with the S_1 surface within the singlet minima with strong spin-orbit coupling (818.1 cm^{-1}, Table S2), meaning that transfer of the singlet onto the triplet energy surface should be thermodynamically favorable. The internal conversion to T_1 should again occur in 10s of ps leading to a T_1 to S_0 emission, with energy ~ 2.919 eV. Because there is only one minimum,

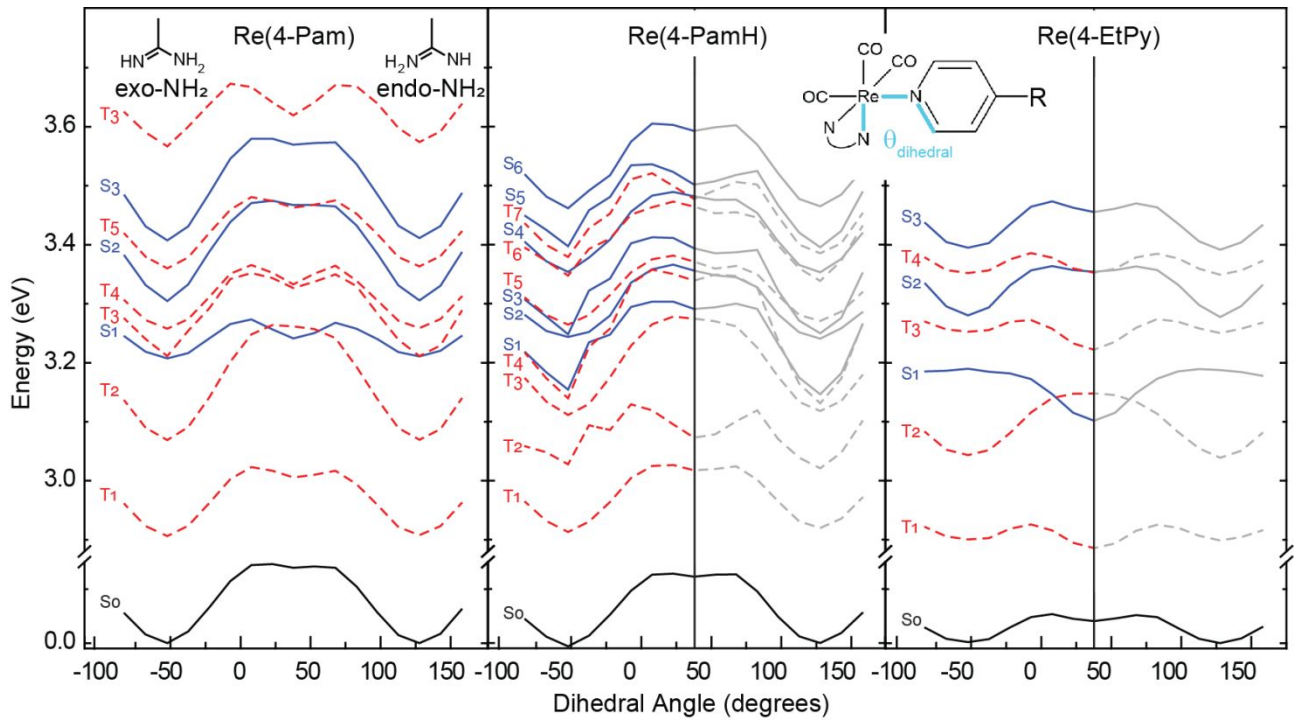

Figure 7. Potential energy curves as a function of the dihedral angle between the pyridine and bpy ligands. The black line (lowest energy curve) is the constrained DFT optimized singlet ground-state surface of each complex. The higher lying, singlet (blue solid lines) and triplet (red dotted lines) potential energy curves are TDDFT excitations from this GS curve. All calculations are B3LYP/LANL2DZ [Re]+6-311G(d,p)[H,C,N,O]/PCM(ACN). (inset) Simplified molecular structure of the rhenium complexes (R = 4-Pam, 4-PamH, 4-EtPy) highlighting the relevant dihedral angle ($\theta_{dihedral}$).

as the molecular structures are equivalent at $\theta_{dihedral}$ = –49° or 126°, there is only one emissive population.

The excited-state evolution the Re(4-EtPy) is similar to that of the Re(4-PamH), in that a single population is excited and evolves through the entire excited-state deactivation. First, excitation occurs from the GS on the Re(4-EtPy) S_0 surface (equivalently at $\theta_{dihedral}$ = –49° or 126°). The S_1 surface of Re(4-EtPy) has a global minimum at $\theta_{dihedral}$ = 45°. The S_1 surface intersects with the T_2 near the singlet minimum with strong spin-orbit coupling between the two (> 700 cm^{-1} 37° – 127°), indicating thermal driving force for transfer into the triplet manifold. After intersystem crossing, the system evolves as a single population, which then deactivates in ~10s of ps to the T_1 surface and then back to the S_0 surface with a lifetime on the order of nanoseconds. The ~ 2.89 eV energy difference between the T_1 and S_0 along the entire PEC as well as the consistently strong coupling (Table S3, > 170 cm^{-1}) are in agreement with the emission wavelengths of the other two complexes.

With these computational results, we are able to provide a framework for understanding the observed experimental results. Re(4-PamH) and Re(4-EtPy) show one emission lifetime because only one population is formed in the emissive excited state (T_1), owing to the symmetry of the 4-PamH and 4-EtPy ligands. In contrast, the 4-Pam ligand is asymmetric around the dihedral angle meaning that it has two rotamers with the same $T_1 \rightarrow S_0$ energy. While these calculations do not reveal the exact nature of the two deactivation pathways that lead to the two observed emission lifetimes, the presence of the matching rotamer emissions indicates that two excited-state populations must evolve at different time-scales.

Non-equilibrated states lead to multiple emission lifetimes: Our work is not the first to report multiple emission lifetimes from transition metal complexes. Typically, when more than one emission lifetime is observed for a pure transition metal complex, the multiple lifetimes arise from non-equilibrated electronic excited states of the complex.

One mechanism that gives rise to the observation of non-exponential photoluminescence is the so-called dual emission mechanism that stems from non-equilibrated excited states. A condition for this mechanism is the presence of two electronic excited states that are very close in energy. Examples of coexisted, non-equilibrated ^{3}MLCT/^{3}ILCT excited states[29] or two distinct ^{3}MLCT excited states[27,31,32] of Ru(II) complexes at room temperature have been reported. ^{3}MLCT/^{3}ILCT type dual emission of carbonyl Re(I) compounds has also been observed at low temperatures.[4] However, such dual emission results in two distinct emission peaks when the non-equilibrated excited states are deactivated. Our experimental and computational results indicate that Re(4-Pam) is not a dual emission system. Re(4-Pam) shows only one emission peak, and TDDFT shows only one low-lying triplet surface, rather than two distinct triplet states or a triplet and quintet that are close in energy.

Other possible rationales to explain the non-exponential photoluminescence behavior of Re(4-Pam), including environmental heterogeneity and structural isomers, have also been considered and discounted. First, while non-exponential kinetics have been reported in rigid or constrained media[28,41] as a result of environmental heterogeneity, our experiments are all solution-based and should not be subject to this effect. Second, the existence of structural isomers in solution can cause non-

exponential kinetics. For Re(I) tricarbonyl molecules, we may expect meridional or facial isomers that could demonstrate similar photoluminescence with different lifetimes. Further, the 4-Pam ligand could bind via the pyridine nitrogen or the nitrogen of the amidine functionality. However, the NMR and IR studies (Supporting Information) indicate that the Re(I) compounds studied in this work are all in the facial configuration and the 4-Pam ligand is only bound through the pyridine nitrogen, which rules out the possibility of metal-centered structural isomers. In addition, ligand photodissociation and subsequent solvent coordination might result in another complex present under photoexcited conditions, however TDDFT of such structures (Figure S13) do not match the steady-state absorption taken before or after the time-resolved measurements, or with the photo-induced absorptions in transient absorption measurements.

The Re(4-Pam) complex reported here shows non-exponential photoluminescence kinetics, however the mechanism underlying this behavior appears to be different than those reported for previous metal complexes. A large geometric change involving an asymmetric ligand results in to two distinct emissive T_1 populations. Because T_1 rotamer minima are approximately the same energy above the S_0, the energy of the emission is essentially the same, and we see only one emission peak.

CONCLUSION

In this work, we present the synthesis and characterization of a new $Re(CO)_3(bpy)(L)$ complex in which L is a 4-pyridyl amidine ligand (4-Pam), Re(4-Pam). The amidine functionality can be protonated to form the protonated 4-PamH and the Re(4-PamH) complex. Steady-state UV-visible and emission spectroscopy of Re(4-Pam) and Re(4-PamH) are in line with expected steady-state spectra based on other Re-carbonyl containing complexes. The similarity is confirmed by comparison to an analogous, previously published L=4-ethylpyridine complex, Re(4-EtPy).

Despite the unremarkable steady-state spectroscopy, the photophysics of the unprotonated Re(4-Pam) are quite unexpected. Rather than one emission lifetime, two lifetimes were observed, along with two corresponding lifetimes observed by transient absorption spectroscopy. In contrast both Re(4-PamH) and Re(4-EtPy) showed only one emission (and one corresponding TAS) lifetime.

We posit that because 4-PamH and 4-EtPy are symmetric ligands, only one excited-state population is formed for Re(4-PamH) and Re(4-EtPy) and one photophysical evolution is observed. Thus, these molecules show only one emission (and corresponding transient absorption lifetime). In contrast, the Re(4-Pam) has two distinct rotamers due to the asymmetry of the 4-Pam ligand, which results in two excited-state populations with the same energy.

DFT and TDDFT rationalize the observed behavior through mapping the potential energy curves of the singlet and triplet excited-state manifolds. The surfaces of Re(4-PamH) and Re(4-EtPy) predict a fast vertical singlet excitation, which thermodynamically undergoes intersystem crossing to the triplet manifold from the lowest singlet excited surface before emission from a single lowest energy triplet minimum. In contrast, Re(4-Pam) has two rotamers which have near identical $T_1 \rightarrow S_0$ emission energies. Two emission lifetimes are experimentally observed for Re(4-Pam), indicating that two triplet populations relax with different rates.

These results are, to the best of our knowledge, the first observation of non-exponential photoluminescence from two excited-state rotamers. Although some previous work has reported the use of proton-sensitive ligands in rhenium(I) tricarbonyl diimine complexes with 1,4-pyrazine ligands[42,43] and with 4,4'-biypridine ligands[44], this field is still relative unexplored and a great deal remains to be discovered. This work describes a new ligand that imparts proton-dependent behavior to the complex and offers computational insight to the nature of the resulting excited state phenomena. This work highlights an interesting new way to control molecular photophysics using a single proton and adds useful insights into the importance of ligand symmetry when designing metal complexes of interest in excited-state proton coupled electron transfer.

EXPERIMENTAL SECTION

Chemicals. All chemicals were purchased from Sigma Aldrich or Alfa Aesar and used without further purification unless noted.

Characterization. ESI-MS data was collected using an Applied Biosystems 3200 Q Trap LC/MS/MS System. 0.4 mL of sample at 1 mg/mL in acetonitrile was added via direct injection to the ionization source. Data was acquired over a range of mass-to-charge ratios (m/z) of 300–900.

UV-visible absorption spectroscopy. Samples for UV-visible absorption spectroscopy were carried out on an Agilent Cary 7000 UV-Vis-NIR Spectrophotometer. Samples were prepared using spectroscopic-grade dicholoromethane that had been dried over KOH for 24 hours. The solvent (1 mL) was transferred in a high-vacuum cuvette with pathlength of 0.4 cm containing approximately 0.25 nmol of the rhenium complex of interest.

Emission spectroscopy. Steady-state and time-resolved emission spectroscopy was carried out on an ISS Chronos BH with steady-state upgrade. Samples for steady-state emission spectroscopy were prepared using spectroscopic-grade dichloromethane that had been dried over KOH for 24 hours. The solvent (1 mL) was transferred in a high-vacuum cuvette with pathlength of 0.4 cm containing 0.25 nmol of the rhenium complex of interest. Samples were degassed using freeze-pump-thaw techniques to ensure that no oxygen was present in the samples. Samples were excited at 370 nm and emission was collected from 450 – 725 nm with 1-nm step-size and 1-second integration time. Excitation spectra were recorded by monitoring the emission at 475 nm, 525 nm, 575 nm, and 625 nm while exciting at wavelengths 290 – 500 nm in 1-nm step-size and 1-second integration time.

Time-resolved emission was recorded with the time-correlated single photon counting configuration of the Chronos BH. An excitation wavelength of 370 nm was used and a 370-nm bandpass filter was used on the excitation channel. A 515-nm longpass filter was used to on the emission channel to ensure that only emission from the Re complexes was collected for the sample and not scattered light from the 370-nm excitation source. The instrument response function was recorded using a dilute solution of coffee creamer in water. The entire emission peak was recorded and integrated to produce the sample signal. The fluorescent lifetimes of each sample were fit to either mono- or bi-exponential decays deconvolved from the instrument response using the provided ISS software.

Electrochemistry. All cyclic voltammetry (CV) measurements were recorded on a CH Instruments potentiostat/galvanostat. CV was performed using a glassy

carbon disk (3-mm diameter) working electrode, a platinum wire counter electrode, and a silver wire quasi reference electrode. The glassy carbon working electrode was polished with 0.05 μM alumina powder/water slurry, rinsed with water and acetone, and allowed to air dry prior to each experiment. Tetrabutylammonium hexafluorophospate ($TBAPF_6$) was recrystallized with hot ethanol three times, dried under vacuum, and used as the supporting electrolyte. Dichloromethane was pre-dried with 3 Å molecular sieves, and stored under N_2 gas prior to use. Ferrocene was used as an internal standard and all voltammograms were reported vs $Fc^{+/0}$ couple. The scan rate used for CV was 100 mV/s unless otherwise specified. All samples were prepared with 0.100 M $TBAPF_6$ and were sparged with N_2 for 10 minutes before CV and DPV and kept under a N_2 blanket during acquisition.

Transient absorption spectroscopy. Femtosecond transient absorption spectroscopy (fs-TA) was performed with an Ultrafast Systems Helios spectrometer. One hundred fifty femtosecond (150-fs) pulses of 800 nm laser light were supplied by a Coherent Libra amplified Ti:sapphire system at 1.1 W and 1 kHz repetition rate. Approximately 80% of the 800 nm pulses was sent to a Topas-C optical parametric amplifier to generate a 370 nm pump pulse. The pump pulse was attenuated to between 0.3 mW and 0.4 mW to prevent decomposition of the sample. The remainder (~20%) of the 800 nm light was used generate a white light continuum for use as the probe pulse. The probe pulse was delayed on a delay stage to generate every other pump pulse, and for each time delay, a series of unpumped and pumped probe pulses were recorded. In each case, a reference probe pulse (that does not go through the sample) was collected and processed to improve the S/N while minimizing the number of scans needed to obtain quality data. The transient absorption spectra were measured over a 5 ns window. For each scan, 250 time points were recorded and each sample was subjected to three scans.

Nano-second transient absorption (ns-TA) was carried out with an Ultrafastsystems EOS spectrometer using the same pump pulse as the fs-TA experiment. However, the probe pulse was generated by a PCF (photonic crystal fiber) based supercontinuum laser. The time window for the experiment was set manually depending on the lifetime of the sample. The time-delay points visited for the experiment were determined by an approximately exponential distribution of delays within the time window that were sampled randomly for the duration of the experimental acquisition. Collection of the pumped and unpumped probe pulses were carried out in the same manner as the Helios experiments. Data was collected and averaged for approximately 45 minutes to generate a completed data set.

Samples were stirred with a magnetic stir bar. Samples for transient absorption spectroscopy were prepared in a 2-mm quartz high-vacuum cuvette at concentrations so that the absorbance at 370 nm was set to an absorption of 0.5 AU. UV-visible absorption spectra were recorded before and after each TA experiment to verify that no decomposition had occurred.

Data analysis was carried out using the Ultrafastsystems Surface Xplorer software that is freely available online. A chirp correction was applied during analysis of each fs-TA data set. Global analysis was performed by extracting and retaining two principal components and fitting using global analysis software package of Surface Xplorer to isolate decay-associated difference spectra (DADS) and their corresponding lifetimes. Quality of the fitting was assessed by examining the residuals of principle component kinetic traces and the model used to represent the dataset.

Computation. Density functional theory (DFT) and time-dependent density functional theory (TDDFT) calculations were performed on all three rhenium complexes in Gaussian09.[45] The B3LYP functional[46–49] and split LANL2DZ[50][Re] and 6-311G(d,p)[51–55][H,C,N,O] basis sets were used. An acetonitrile solvent environment was simulated with the complete polarizable continuum model (PCM) of acetonitrile. The fully optimized structure of the singlet ground and lowest triplet state for each molecule were calculated and confirmed at true minima with no imaginary frequencies. The frontier molecular orbitals (Figure S4) for singlet and triplet states were produced using GaussView 6.[56] The lowest energy singlet and triplet surface (Figure S6) was sampled through a scan of the N(bpy)-Re-N(4-Pam)-C dihedral angle in increments of 15° (210° forward and 30° backward from the GS). TDDFT singlets and triplets were performed at each geometry on the lowest energy singlet surface (Figure 7). The one-electron Z_{eff} spin-orbit couplings were tabulated using a modified PySOC[57] where the Re^{2+} was assigned a Z_{eff} = 1078.5.[58]

ASSOCIATED CONTENT

Supporting Information. Detailed synthetic procedures, IR spectrum, NMR spectra, ESI-MS spectrum, time-resolved photoluminescence (tr-PL), temperature-dependent tr-PL, transient absorption data and fitting, DFT optimized geometries and TDDFT excitation tables are provided in the Supporting Information. This material is available free of charge via the Internet at http://pubs.acs.org.

AUTHOR INFORMATION

Corresponding Author

*Email: ery317@lehigh.edu; Fax: +1-610-758-6536.

Author Contributions

The manuscript was written through contributions of all authors. All authors have given approval to the final version of the manuscript.

Funding Sources

National Science Foundation CHE-1428633.

ACKNOWLEDGMENT

The authors thank the NSF Major Research Instrumentation program (CHE-1428633) for funding that established the laser facility. This work made use of the Lehigh University NMR Facility. The Bruker Neo 500 MHz NMR was acquired through NSF-MRI-1725883, with additional support from Lehigh University.

ABBREVIATIONS

DFT, Density Functional Theory; TDDFT, Time-Dependent Density DFT; MO, molecular orbitals; HOMO, highest occupied molecular orbital; LUMO, lowest unoccupied molecular orbital; TAS, transient absorption spectroscopy.

REFERENCES

1 D. M. Arias-Rotondo and J. K. McCusker, *Chemical Society Reviews*, 2016, 5803–5820.
2 J. K. McCusker, *Science*, 2019, 484–488.
3 A. Ramdass, V. Sathish, E. Babu, M. Velayudham, P. Thanasekaran

and S. Rajagopal, *Coordination Chemistry Reviews*, 2017, **343**, 278–307.
4 A. I. Baba, J. R. Shaw, J. A. Simon, R. P. Thummel and R. H. Schmehl, *Coordination Chemistry Reviews*, 1998, **171**, 43–59.
5 K. Kalyanasundaram, *Coordination Chemistry Reviews*, 1982, **46**, 159–244.
6 D. W. Thompson, A. Ito and T. J. Meyer, *Pure and Applied Chemistry*, 2013, **85**, 1257–1305.
7 J. V. Caspar, T. D. Westmoreland, G. H. Allen, T. J. Meyer, P. G. Bradley and W. H. Woodruff, *Journal of the American Chemical Society*, 1984, **106**, 3492–3500.
8 T. J. Meyer, *Pure and Applied Chemistry*, 1986, **58**, 1193–1206.
9 J. V. Caspar and T. J. Meyer, *Inorganic Chemistry*, 1983, **22**, 2444–2453.
10 J. V Caspar and T. J. Meyer, *The Journal of Physical Chemistry*, 1983, **6**, 952–957.
11 G. H. Allen, R. P. White, D. P. Rillema and T. J. Meyer, *Journal of the American Chemical Society*, 1984, 2613–2620.
12 V. Komreddy, K. Ensz, H. Nguyen, D. P. Rillema and C. E. Moore, *Journal of Molecular Structure*, 2020, **1223**, 128739.
13 H. S. Liew, C. W. Mai, M. Zulkefeli, T. Madheswaran, L. V. Kiew, N. Delsuc and M. Lee Low, *Molecules*, 2020, **25**, 4176.
14 V. Komreddy, K. Ensz, H. Nguyen and P. D. Rillema, *Inorganica Chimica Acta*, 2020, **511**, 119815.
15 E. Wolcan, *Inorganica Chimica Acta*, 2020, **509**, 119650.
16 T. P. Nicholls, L. K. Burt, P. V. Simpson, M. Massi and A. C. Bissember, *Dalton Transactions*, 2019, **48**, 12749–12754.
17 B. Merillas, E. Cuéllar, A. Diez-Varga, T. Torroba, G. García-Herbosa, S. Fernández, J. Lloret-Fillol, J. M. Martín-Alvarez, D. Miguel and F. Villafañe, *Inorganic Chemistry*, 2020, **59**, 11152–11165.
18 R. Fernández-Terán and L. Sévery, *Inorganic Chemistry*, 2021, **30**, 1334–1343.
19 J. Mukherjee and I. Siewert, *European Journal of Inorganic Chemistry*, 2020, 4319–4333.
20 Y. Kuramochi and A. Satake, *Chemistry - A European Journal*, 2020, **26**, 16365–16373.
21 D. A. Kurtz, K. R. Brereton, K. P. Ruoff, H. M. Tang, G. A. N. Felton, A. J. M. Miller and J. L. Dempsey, *Inorganic Chemistry*, 2018, **57**, 5389–5399.
22 L. Sacksteder, A. P. Zipp, E. A. Brown, J. Streich, J. N. Demas and B. A. DeGraff, *Inorganic Chemistry*, 1990, **29**, 4335–4340.
23 G. Tapolsky, R. Duesing and T. J. Meyer, *Journal of Physical Chemistry*, 1991, **95**, 1105–1112.
24 D. S. English, R. L. Rich and J. W. Petricht, *Photochemistry and Photobiology*, 1998, **67**, 76–83.
25 J. W. Petrich, M. C. Chang, D. B. McDonald and G. R. Fleming, *Journal of the American Chemical Society*, 1983, **105**, 3824–3832.
26 W. B. De Lauder and P. Wahl, *Biochemistry*, 1970, **9**, 2750–2754.
27 D. Magde, M. D. Magde and E. C. Glazer, *Coordination Chemistry Reviews*, 2016, **306**, 447–467.
28 T. A. Heimer and G. J. Meyer, *Journal of Luminescence*, 1996, **70**, 468–478.
29 L. Song, J. Feng, X. Wang, J. Yu, Y. Hou, P. Xie, B. Zhang, J. Xiang, X. Ai and J. Zhang, *Inorganic Chemistry*, 2003, **42**, 3393–3395.
30 T. E. Keyes, *Chemical Communications*, 1998, 889–890.
31 E. C. Glazer, D. Magde and Y. Tor, *Journal of the American Chemical Society*, 2007, **129**, 8544–8551.
32 E. C. Glazer, D. Magde and Y. Tor, *Journal of the American Chemical Society*, 2005, **127**, 4190–4192.
33 M. R. Camilo, C. R. Cardoso, R. M. Carlos and A. B. P. Lever, *Inorganic Chemistry*, 2014, **53**, 3694–3708.
34 Q. Zhang, H. Kuwabara, W. J. Potscavage, S. Huang, Y. Hatae, T. Shibata and C. Adachi, *Journal of the American Chemical Society*, 2014, **136**, 18070–18081.
35 M. C. Chang, J. W. Petrich, D. B. Mcdonald and G. R. Fleming, *Journal of the American Chemical Society*, 1983, **105**, 3819–3824.
36 T. E. Knight, D. Guo, J. P. Claude and J. K. Mccusker, *Inorganic Chemistry*, 2008, **47**, 7249–7261.
37 I. Favier and E. Duñach, *Tetrahedron Letters*, 2004, **45**, 3393–3395.
38 D. Ung, *Doctoral Thesis*, 2020, https://digital.lib.washington.edu/researchworks/h.
39 T. J. Penfold, E. Gindensperger, C. Daniel and C. M. Marian, *Chemical Reviews*, 2018, **118**, 6975–7025.
40 L. A. Fredin and P. Persson, *The Journal of Physical Chemistry A*, 2019, **123**, 5293–5299.
41 D. W. Thompson, C. N. Fleming, B. D. Myron and T. J. Meyer, *The Journal of Physical Chemistry B*, 2007, **111**, 6930–6941.
42 C. Bronner and O. S. Wenger, *Inorganic chemistry*, 2012, **51**, 8275–8283.
43 O. S. Wenger, *Chemistry - A European Journal*, 2011, **17**, 11692–11702.
44 P. Dongare, A. G. Bonn, S. Maji and L. Hammarström, *Journal of Physical Chemistry C*, 2017, **121**, 12569–12576.
45 M. J. Frisch, G. W. Trucks, H. B. Schlegel, G. E. Scuseria, M. A. Robb, J. R. Cheeseman, G. Scalmani, V. Barone, G. A. Petersson, H. Nakatsuji, X. Li, M. Caricato, A. V. Marenich, J. Bloino, B. G. Janesko, R. Gomperts, B. Mennucci, H. P. Hratchian, J. V. Ortiz, A. F. Izmaylov, J. L. Sonnenberg, D. Williams-Young, F. Ding, F. Lipparini, F. Egidi, J. Goings, B. Peng, A. Petrone, T. Henderson, D. Ranasinghe, V. G. Zakrzewski, J. Gao, N. Rega, G. Zheng, W. Liang, M. Hada, M. Ehara, K. Toyota, R. Fukuda, J. Hasegawa, M. Ishida, T. Nakajima, Y. Honda, O. Kitao, H. Nakai, T. Vreven, K. Throssell, J. J. A. Montgomery, J. E. Peralta, F. Ogliaro, M. J. Bearpark, J. J. Heyd, E. N. Brothers, K. N. Kudin, V. N. Staroverov, T. A. Keith, R. Kobayashi, J. Normand, K. Raghavachari, A. P. Rendell, J. C. Burant, S. S. Iyengar, J. Tomasi, M. Cossi, J. M. Millam, M. Klene, C. Adamo, R. Cammi, J. W. Ochterski, R. L. Martin, K. Morokuma, O. Farkas, J. B. Foresman and D. J. Fox, 2016, Gaussian 16, Gaussian, Inc., Wallingford CT.
46 R. Ditchfield, W. J. Hehre and J. A. Pople, *The Journal of Chemical Physics*, 1971, **54**, 724–728.
47 M. M. Francl, W. J. Pietro, W. J. Hehre, J. S. Binkley, M. S. Gordon, D. J. DeFrees and J. A. Pople, *The Journal of Chemical Physics*, 1982, **77**, 3654–3665.
48 W. J. Hehre, R. Ditchfield and J. A. Pople, *The Journal of Chemical Physics*, 1972, **56**, 2257–2261.
49 P. C. Hariharan and J. A. Pople, *Theoretica Chimica Acta*, 1973, **28**, 213–222.
50 Y. Yang, M. N. Weaver and J. Kenneth M. Merz, *Journal of Physical Chemistry A*, 2009, **113**, 9843–9851.
51 A. D. Becke, *The Journal of Chemical Physics*, 1993, **98**, 5648–5652.
52 C. Lee, W. Yang and R. G. Parr, *Physical Review B*, 1988, **37**, 785–789.
53 S. H. Vosko, L. Wilk and M. Nusair, *Canadian Journal of Physics*, 1980, **58**, 1200–1211.
54 P. J. Stephens, F. J. Devlin, C. F. Chabalowski and M. J. Frisch, *Journal of Physical Chemistry*, 1994, **98**, 11623–11627.
55 F. Weigend, M. Häser, H. Patzelt and R. Ahlrichs, *Chemical Physics Letters*, 1998, **294**, 143–152.
56 R. Dennington, T. Keith and J. Millam, 2016, GaussView, Version 6; Semichem Inc., Shawnee Missi.
57 X. Gao, S. Bai, D. Fazzi, T. Niehaus, M. Barbatti and W. Thiel, *Journal of Chemical Theory and Computation*, 2017, **13**, 515–524.
58 S. Koseki, M. W. Schmidt and M. S. Gordon, *Journal of Physical Chemistry A*, 1998, **102**, 10430–10435.

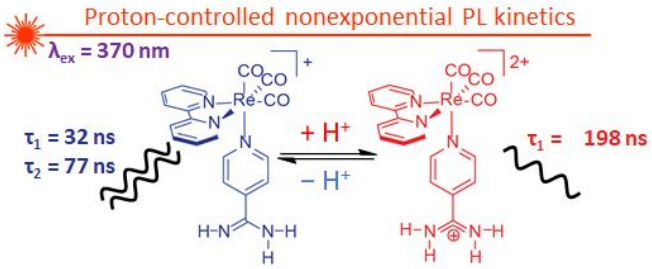
Proton-controlled nonexponential PL kinetics
λex = 370 nm
τ1 = 32 ns
τ2 = 77 ns
+ H+
– H+
τ1 = 198 ns